J IRAN CHEM SOC (2017) 14:1815–1826
DOI 10.1007/s13738-017-1121-1

ORIGINAL PAPER

Quantum dynamics of electron capture process during H–He^{2+} collision

Hassan Sabzyan[1] · **Mohammad Jafar Jenabi**[1]

Received: 21 October 2016 / Accepted: 13 April 2017 / Published online: 25 April 2017

Abstract Quantum dynamics of electron transfer (capture) phenomenon during the H–He^{2+} collision is investigated by solving two-dimensional time-dependent Schrödinger equation numerically using a third-order split operator technique. Results of this study, represented as the snapshots of the electron wavepacket time evolution, show significantly different dynamics for the electron of different initial orbitals (1*s*, 2*s*, $2p_x$ and $2p_y$) of the incoming hydrogen atom. This electron transfer dynamics is also detailed by calculating expansion coefficients of the projection of the evolving wavepacket onto the stationary eigenfunctions of the H and He^+ species to investigate evolution of the electron density around each nucleus during the collision. The instantaneous and overall electron densities captured by the He^{2+} nucleus from the H atom are calculated and analyzed. It is also shown evidently and concluded that due to its quantum nature, electron crawls from one nucleus to the other in an electron transfer process during an atom–ion collision.

Keywords Electron transfer · Electron capture · Time-dependent Schrödonger equation · Atom-ion collision · Quantum dynamics

Introduction

The ion–molecule, ion–atom and ion–ion collisions are classified into two main elastic and inelastic categories depending on the outcome of the collision. In the elastic scattering, the colliding species are deflected from their original paths without any changes in their internal energies, while in the inelastic collision or scattering, a number of exit channels are possible, including (1) excitation or ionization of one or both colliding species, (2) reactive scattering in which the two colliding species may attach to each other, decompose into smaller species, abstract atom(s) from each other, or even exchange atom(s) and (3) electron transfer (or capture), in which one or more electrons are transferred from one to the other species. Emission of radiation may also be an outcome of any of these inelastic scattering channels. Similar channels can be considered for the collision of atomic charged and/or neutral species, except for the inelastic reactive channel which is limited to the attachment reactions only. A charge exchange or electron transfer process between two particles (e.g., $A^0 + B^+ \rightarrow A^+ + B^0$) may also be viewed as either an electron loss or an electron gain (capture) process depending on the choice of the reference particle (A^0 or B^+). Therefore, *charge exchange*, *electron transfer* and *electron capture* are alternatively used in this context for the electron transfer inelastic channel (3).

Electron capture process has been a fascinating topic for physicists and chemists. This process covers a wide range of phenomena from simple electrostatics to complex chemical reactivities and mechanisms in solutions and charge exchange and reactions at the interfaces [1, 2]. Almost a century ago, Flamm and Schumann [3] suggested that an alpha particle may capture an electron from the penetrated medium. About a decade later, presence of singly charged helium ions, presence of He^+ (i.e., electron captured alpha particles) in the α beam emerging from radioactive samples was demonstrated experimentally by Henderson [4], Rutherford [5] and Jacobsen [6], independently. It was then concluded that electron capture must be possible for all

✉ Hassan Sabzyan
sabzyan@sci.ui.ac.ir

[1] Department of Chemistry, University of Isfahan, Isfahan 81746-73441, Islamic Republic of Iran

charged particles and ions, including protons, when passing through a medium or encountering another particle. Since then, the charge exchange processes have also been identified and extensively studied in the chemical and biological systems, such as photosynthesis and redox reactions in solutions and electrochemical reactions at the electrode surfaces, as well as electron transfer across semiconductor junctions [7–9]. A variety of electron transfer-related phenomena, such as low-temperature, nuclear tunneling and dissociative electron transfer, has so far been identified in the electrochemical type of charge transfer [10–13]. Different theoretical methods have been used to study details of electron capture phenomenon. Investigation of low-energy collisions such as the perturbed stationary state model, molecular orbital model and Landau–Zener–Stückelberg approximation, and high-energy collisions such as Oppenheimer–Brinkman–Kramers, boundary-corrected first Born (BIB), the continuum-distorted wave (CDW), and the Eikonal approximations and the Thomas double-scattering mechanism are examples of electron capture studies [14–16].

In the first step of this series of works carried out in our research group, electron transfer during the interaction of a hydrogen atom and ions (bare nuclei) of different charges has been studied quantum mechanically by solving time-dependent Schrödinger equation (TDSE) considering fixed nuclei [17]. It was shown that the extent of electron transfer depends on the charges of the two nuclei and their distance, which are parameters of the potential governing evolution of the electron wavepacket. Here in this work, details of the quantum dynamics of the electron transfer (capture) phenomenon during a realistic collision between a hydrogen atom and an α particle, i.e., in the H–He^{2+} system, in which both particles are free to move are worked out without using soft-core potential. To our knowledge, time evolution of the ET process has been studied only for the Li^{+}-Na($3s$,$3p$) collision system using a semiclassical model with molecular basis functions [18].

Theoretical model and computations

Evolution of the electron wavepacket $\Psi(\boldsymbol{r},t)$ is followed quantum mechanically by solving time-dependent Schrödinger equation (TDSE) given in atomic units as

$$\imath \frac{\partial}{\partial t}\Psi(\boldsymbol{r},t) = \hat{H}(\boldsymbol{r},t)\Psi(\boldsymbol{r},t) \tag{1}$$

in which $\imath = \sqrt{-1}$ and $\hat{H}(r,t)$ are the Hamiltonian operator of the system, defined as the sum of kinetic $\hat{T} = \sum_j T_j = -\sum_j (P_j^2/2m_j)$ and potential $\hat{V} = \sum_j \hat{V}_j + \sum_{i,j} \hat{V}_{ij}$ energy operators. Here, m_j and P_j are the mass and momentum of the particle j. The potential energy operator includes all particle–field ($\hat{V}_j$) and particle–particle ($\hat{V}_{ij}$) interactions. In the present model, no external field has been considered, and thus, the potential energy operator includes only the pair-wise interactions. For our two-dimensional H–He^{2+} system, we have:

$$\begin{aligned}\hat{T} = &-\frac{1}{2m_e}\left(P_{e,x}^2 + P_{e,y}^2\right) - \frac{1}{2m_p}\left(P_{p,x}^2 + P_{p,y}^2\right) \\ &- \frac{1}{2m_\alpha}\left(P_{\alpha,x}^2 + P_{\alpha,y}^2\right)\end{aligned} \tag{2}$$

$$\begin{aligned}\hat{V} = &-\frac{1}{\sqrt{\left(x_e - x_p\right)^2 + \left(y_e - y_p\right)^2}} \\ &- \frac{2}{\sqrt{\left(x_e - x_\alpha\right)^2 + \left(y_e - y_\alpha\right)^2}} \\ &+ \frac{2}{\sqrt{\left(x_\alpha - x_p\right)^2 + \left(y_\alpha - y_p\right)^2}}\end{aligned} \tag{3}$$

in which the subscripts e, p and α denote the electron, proton (H^+) and α particle (He^{2+}), respectively. The instantaneous evolution of the electronic wavepacket at each time instance t, i.e., from $\Psi(\boldsymbol{r},t)$ to $\Psi(\boldsymbol{r},t+\tau)$, is obtained using the time propagator technique, given by

$$\Psi(\boldsymbol{r},t+\tau) = \hat{U}(\boldsymbol{r},\tau)\Psi(\boldsymbol{r},t) \tag{4}$$

where τ is the time step and is very small compared to the whole process timescale. In this research, propagator operator $\hat{U}(\tau)$ is evaluated using a third-order split operator technique [19–24] proposed by Feynman [25] defined as

$$\begin{aligned}\hat{U}(\boldsymbol{r},\tau) = exp\left(-\imath\tau\hat{H}\right) \approx exp\left(-\imath\tau\hat{V}/2\right) \\ exp\left(-\imath\tau\hat{T}\right)exp\left(-\imath\tau\hat{V}/2\right)\end{aligned} \tag{5}$$

This split operator scheme has an error of the order of τ^3 which gives, therefore, accurate and acceptable results. In general, the split operator method is unitary and conserves the norm of the initial state [26].

The electron dynamics during the H-α (H–He^{2+}) collision is simulated by solving time-dependent Schrödinger equation described in introduction section using a third-order split operator technique. The motions of nuclei p and α (described by the last two terms of the kinetic and the last term of the potential energy operators) are treated classically using Verlet algorithm [27, 28] based on the corresponding forces evaluated after each step of the evolution of electronic wavepacket. Therefore, the corresponding terms are omitted from the Hamiltonian operator when following the motion of electron.

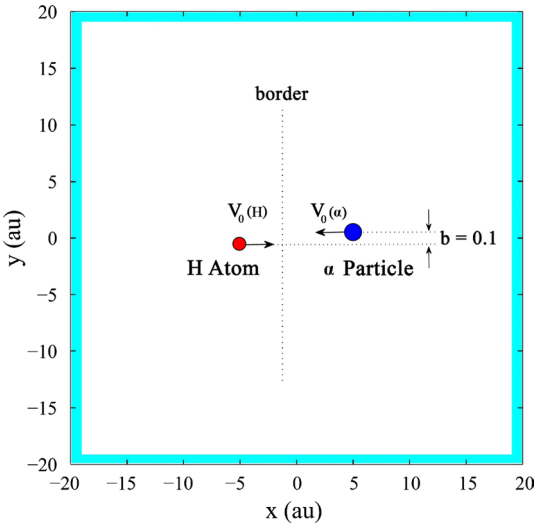

Fig. 1 Setup of the simulation box used for the study of quantum dynamics of electron capture process in an H-α (H–He^{2+}) collision. The *vertical dotted line* passing through the force null point on the internuclear axis shows the border of the two regional densities belonging to the two nuclei, defined as $f_H(r = r_{null}) = f_\alpha(r = r_{null})$. The absorbing imaginary potential on the borders of the simulation box is shaded in *cyan*. The two colliding species are located symmetrically around the box center with vertical (impact parameter) and horizontal distances of 0.1 au and 10, and initial horizontal velocities of 0.5 au

The simulation box used in the present study, demonstrated in Fig. 1, has 40 × 40 au dimensions with an absorbing Heaviside form potential strip of 1 au width at its borders to avoid unphysical reflections of the wavepacket from the walls [29, 30].

Calculations are carried out in the laboratory-fixed frame located at the center of the simulation box. A mesh size of $N = 2048$ (i.e., $\Delta x \approx 0.02$ au) is used to grid the simulation box. The time step (τ) is set to 0.01 au. The two colliding species, a hydrogen atom and an α particle, are located symmetrically around the box center, respectively, at ($x_{p,0} = -5.00$, $y_{p,0} = -0.05$ au) and ($x_{\alpha,0} = 5.00$, $y_{\alpha,0} = +0.05$) which gives a distance of ~10.00 au and an initial impact parameter of 0.10 au. Both nuclei are set to move (classically) toward each other along the horizontal (x) axis with initial velocities of $V_{p,x} = 0.50$ au and $V_{\alpha,x} = -0.50$ au (i.e., with a relative velocity of 1.00 au) already used in the relevant ion–atom experimental works [14, 31].

Results and discussion

The electron transfer process starts with the setup demonstrated in Fig. 1. The electron is initially in one of the two-dimensional (2D) 1*s*, 2*s*, $2p_x$ and $2p_y$ orbitals of the hydrogen atom [32] following the motion of its nucleus (i.e., proton) while evolving under the influence of both nuclear attractors.

The end of the course of electron transfer process is considered to be the time at which the two nuclei take a 20 au distance from each other after their collision. This long-distance criterion is set to make sure that the charge exchange process is reached its asymptotic state. This state depends on a number of physical conditions such as initial positions of the nuclei and their velocities.

The probability density associated with the evolving wavepacket of the single electron of this H–He^{2+} system over the space of the simulation box is calculated at each time instance t during the course of interaction. The time evolution of the system is realized by following variation of this probability density in two ways, contour maps and three-dimensional surfaces. For brevity, only a few snapshots of this evolution, representing the whole evolution process adequately, are presented in this report.

The results obtained for the electron capture process when stating with the 2D hydrogen atom in its 1*s* orbital are plotted in Fig. 2. As shown in Fig. 2a, at $t = 7$ au after triggering the simulation, when the two species reach a distance of ~3.0 au from one another in their approach toward the encounter (collision) center, disturbance of the electron cloud around the hydrogen nucleus, due to the presence of the α particle, becomes evident. Significant partial electron capture by the α particle from the hydrogen atom starts at time $t = 8$ au. Furthermore, at time $t = 9.05$ au, the two approaching species reach their minimum distance (i.e., 0.12 au, which is found by following the internuclear distance as a function of time) which can be regarded as the collision time. At time $t = 12$ au, the charge exchange process is almost completed. In the early stage of the encounter, the electron wavepacket is slightly attracted and distorted by the α particle which results in increasingly faster evolution of the electron wavepacket from the hydrogen nucleus toward the α particle, while the partially stripped hydrogen nucleus is decelerated due to the repulsion interaction with the α particle.

In Fig. 2b, the same results are presented from a side-view (along the x-axis) perspective which contains more details of the wavepacket evolution. For better resolution of the details of this electron transfer process from this perspective, the highest peaks of the wavepacket probability density at all times are scaled all to unity with a factor given inside each plot. It should also be noted that, the color scale in each frame is assigned based on the maximum and minimum values of the wavepacket probability density in the corresponding time step. It is shown in Fig. 2b that how electron evolves toward the alpha particle before the collision time. An interesting feature of this electron capture process can be seen at $t = 10$ at

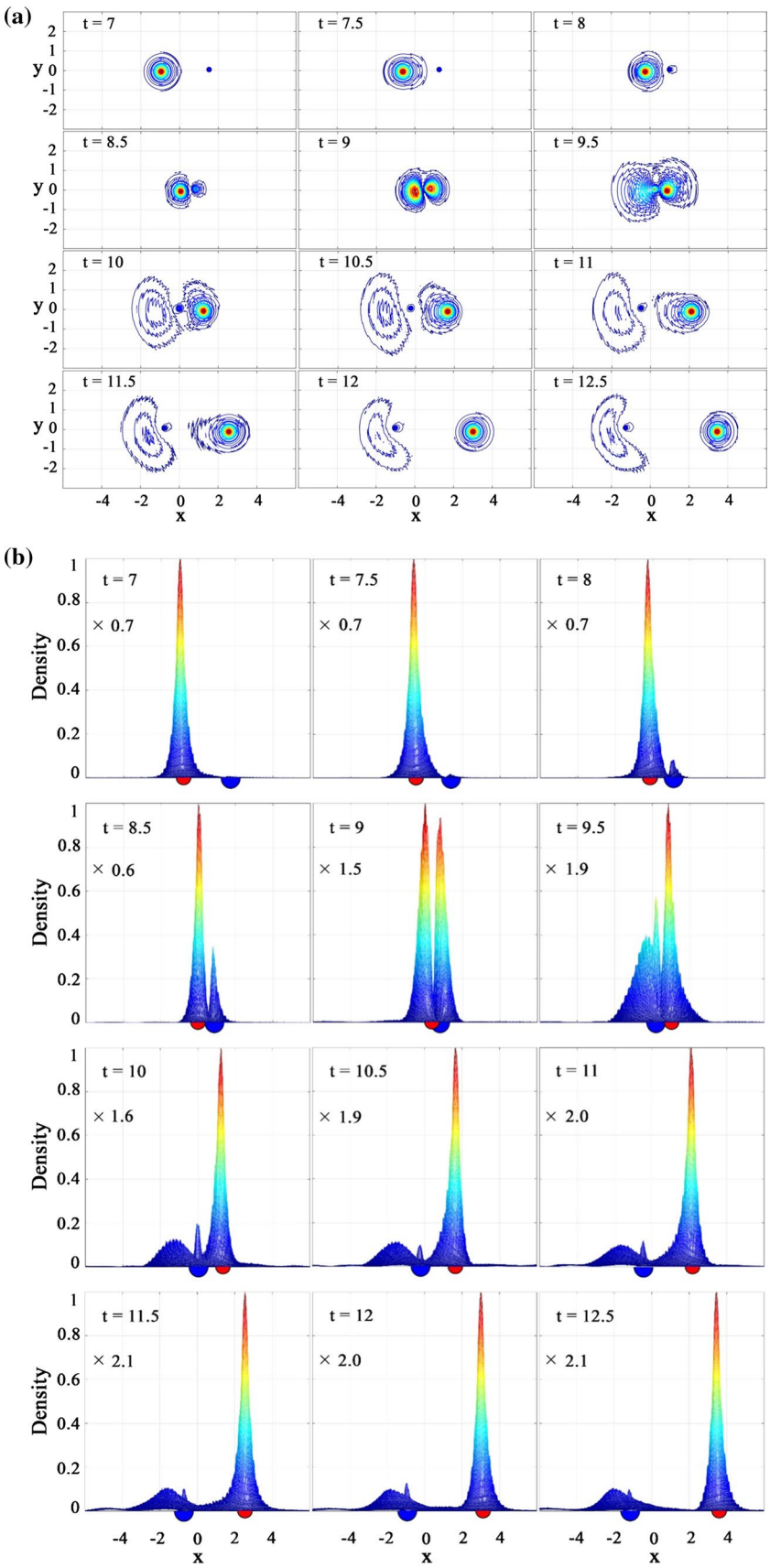

Fig. 2 **a** Contour plots of the snapshots of the evolving electron wavepacket describing the electron capture process in an H-α (H–He^{2+}) collision in the simulation box and conditions given in Fig. 1, when electronic state of the incoming H atom is the 1*s* orbital. In these plots, the H atom and α particle are represented by *red* and *blue circles*, respectively. **b** The side-view plots corresponding to the contour plots are given in part (**a**)

which electron wavepacket has evolved beyond the alpha particle.

After $t = 12.5$ au (not shown in Fig. 2), the α particle grabs the electron of the hydrogen atom partially and continues its trajectory accompanied by the captured part of the electron wavepacket. Up to $t = 21.0$ au, the captured part of the wavepacket is not settled down to the orbitals (eigenfunctions) of the He^+ particle and is distributed asymmetrically around its nucleus and is more spread out as compared to the remaining part of the electron wavepacket which is distributed more or less symmetrically around the proton (i.e., nucleus of the hydrogen atom). At times longer than $t = 24$ au, distribution of the captured electron wavepacket around the α particle becomes almost symmetric, still not settled down in the He^+ orbitals.

Evolution of the wavepacket during electron transfer process when the incoming 2D hydrogen atom is in its $2s$ orbital is presented in Fig. 3. It is shown in this figure that evolution of the electron in this orbital as a result of the H–He^+ interaction is more intense due to its higher energy and farther distribution of the two-peak electron density from the H nuclei, as compared to that of the lower energy and one-peak more compact electron density of the $1s$ orbital. In addition, at longer times after the collision, part of the evolving electron wavepacket has scattered away from both nuclei all over the simulation box.

The results obtained for the $2p_x$ and $2p_y$ orbitals are demonstrated in Figs. 4 and 5, respectively. Comparison between Figs. 3 and 4 shows that the $2p_x$ electron is scattered less than the $2s$ electron during the H–He^{2+} collision due to more concentration of the $2p_x$ orbital around the internuclear axis and its more compact distribution around the H nucleus, as compared to that of the $2s$ orbital. Analysis of snapshots of Fig. 4 shows that evolution of the $2p_x$ orbital of the H atom occurs in two distinct stages corresponding to the sequential encounter of its two right and left lobes with the He^{2+} nucleus. The main scattered electron wavepacket comes from the right lobe of the $2p_x$ orbital which encounter the alpha particle earlier at time ~5 au, as compared to the late encounter of the left lobe after the collision time ($t > 10$ au) which evolves around the He^{2+} nucleus even up to the $t = 27$ au time.

One interesting feature of these simulations, which are carried out at 0.5 au velocities of both particles parallel to x-axis, corresponding to a relative velocity of 1.0 au in the same direction, is that electron of the H atom in its second layer ($2s$, $2p_x$ and $2p_y$ orbitals) lags behind its nucleus. This feature is shown in Figs. 3, 4 and 5 at times before collision (e.g., $t = 5$ au) clearly. This lagging follows the order $2p_y > 2p_x > 2s$. Lagging of electron behind its carrier nucleus slightly affects picture of the wavepacket evolution and its consequent outcome of the electron transfer process and may be neglected at smaller velocities. This interesting phenomenon deserves an independent study which has not been our focus in this work.

Evolution of the wavepacket during electron transfer process when the incoming hydrogen atom is in its $2p_y$ orbital (Fig. 5) is distinctly different from those of the $2s$ and $2p_x$ orbitals described above in that it scatters less. Furthermore, it seems that a major part of the electron wavepacket is carried away from the collision center by the alpha particle neatly in its $2p_y$ orbital. This behavior can be justified by inspecting the trajectory of the alpha particle which shows that it passes through the low-density part of the $2p_y$ orbital near the H nucleus. This passage allows the alpha particle to grab the $2p_y$ electron in a competition with the H nucleus before significantly disturbing its probability density distribution (Fig. 5, $t = 27$ au). It can be predicted that other initial setups, e.g., larger values of impact parameter, will result in a totally different evolutions similar to what observed for the $2p_x$ and $2s$ orbitals.

Details of the instantaneous evolution of the wavepacket (WP) from one (the H) nucleus to the other (alpha particle) can be visualized by projecting it onto the stationary orbitals $\Psi_j\left(\boldsymbol{r}-\boldsymbol{r_p}(t);z=1\right)$ and $\Psi_k(\boldsymbol{r}-\boldsymbol{r_\alpha}(t);z=2)$, respectively, of the original possessor (H) and the grabber (He^+) species as

$$WP=\sum_{j\in H}c_j(t)\Psi_j(\boldsymbol{r}-\boldsymbol{r_H}(t);z=1)+\sum_{k\in He^+}d_k(t)\Psi_k(\boldsymbol{r}-\boldsymbol{r_\alpha}(t);z=2) \tag{6}$$

A nonzero value of expansion coefficients $c_j(t)$ indicates excitation of the electron from its initial state $\Psi_i\left(\boldsymbol{r}-\boldsymbol{r_p}(0);z=1\right)$ on the H atom to its higher states $\Psi_j\left(\boldsymbol{r}-\boldsymbol{r_p}(t);z=1\right)$ with $i\neq j$, as the transient states, while a nonzero value of $d_k(t)$ denotes electron transfer from the H atom to the $\Psi_k(\boldsymbol{r}-\boldsymbol{r_\alpha}(t);z=2)$ state of the He^+ species. This projection is carried out for all four simulations described above, and the resulting time-dependent expansion coefficients $c_j(t)$ and $d_k(t)$ are plotted in Fig. 6, in red and blue, respectively. For better visibility, some $d_k(t)$ coefficients are multiplied by appropriate factors as indicated on the corresponding curves.

Analysis of the expansion coefficients plotted in Fig. 6a shows that when the starting state of the H atom is $1s$ orbital, the residual electron density on the H atom mainly has a $1s$ character. This feature is evident in both parts of Fig. 2 up to $t = 12.5$ au. Furthermore, electron transfer from the $1s$ orbital of the H atom occurs mainly to the $2p_x$, $2s$ and $3d_{x^2-y^2}$ orbitals of the He^+ species. It is interesting that even the $1s$ orbital of the He^+ species has a small transient contribution to the evolving wavepacket of the transferring electron.

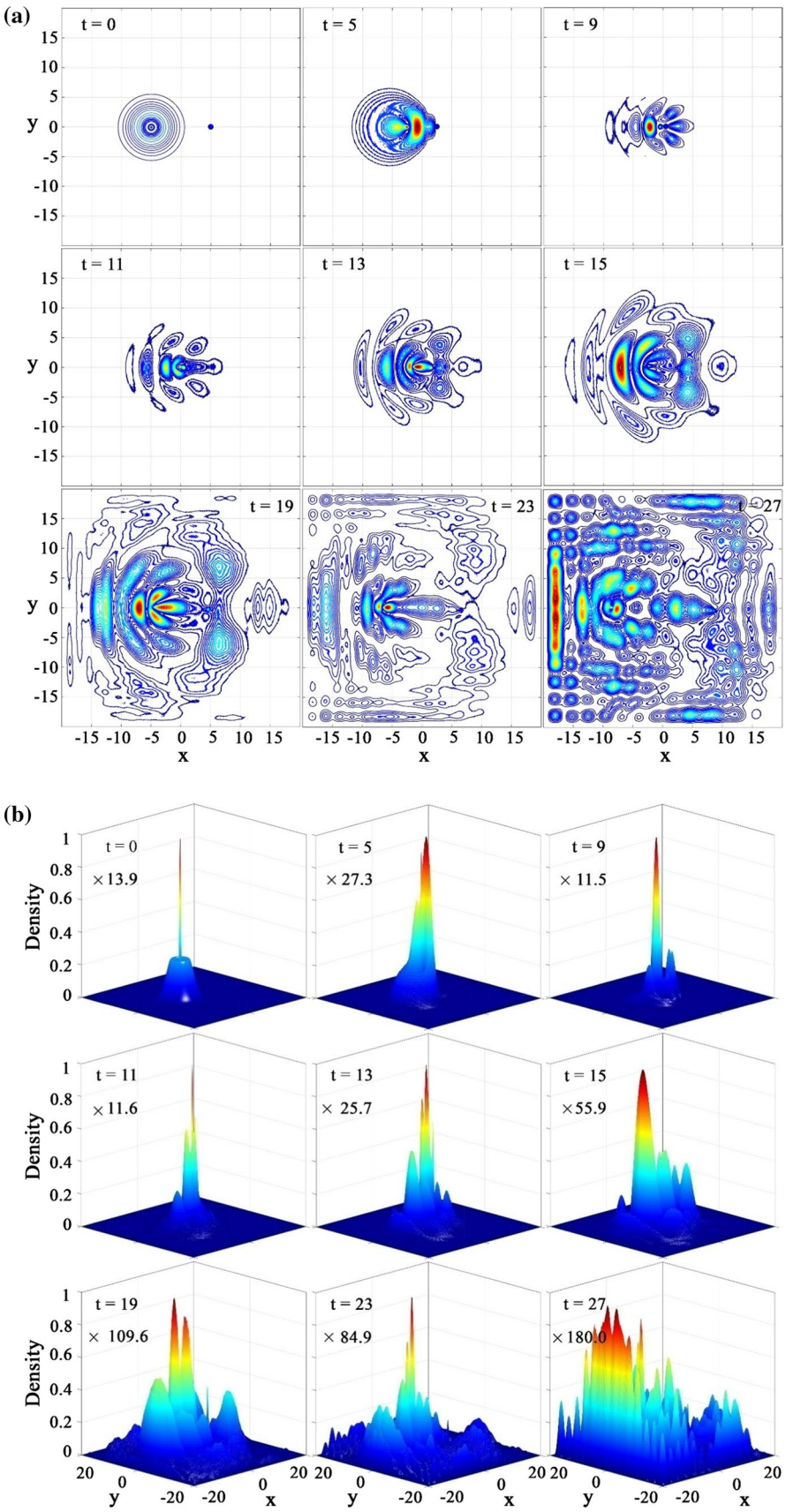

Fig. 3 **a** Contour plots of the snapshots of the evolving electron wavepacket showing electron capture process in an H–He^{2+} collision in the simulation box and conditions demonstrated in Fig. 1, when electron of the incoming H atom is in its 2*s* orbital. In these plots, the H atom and α particle are represented by *red* and *blue circles*, respectively. **b** Snapshots of the evolving wavepacket 3D surface corresponding to the contour plots demonstrated in part (**a**) of this figure

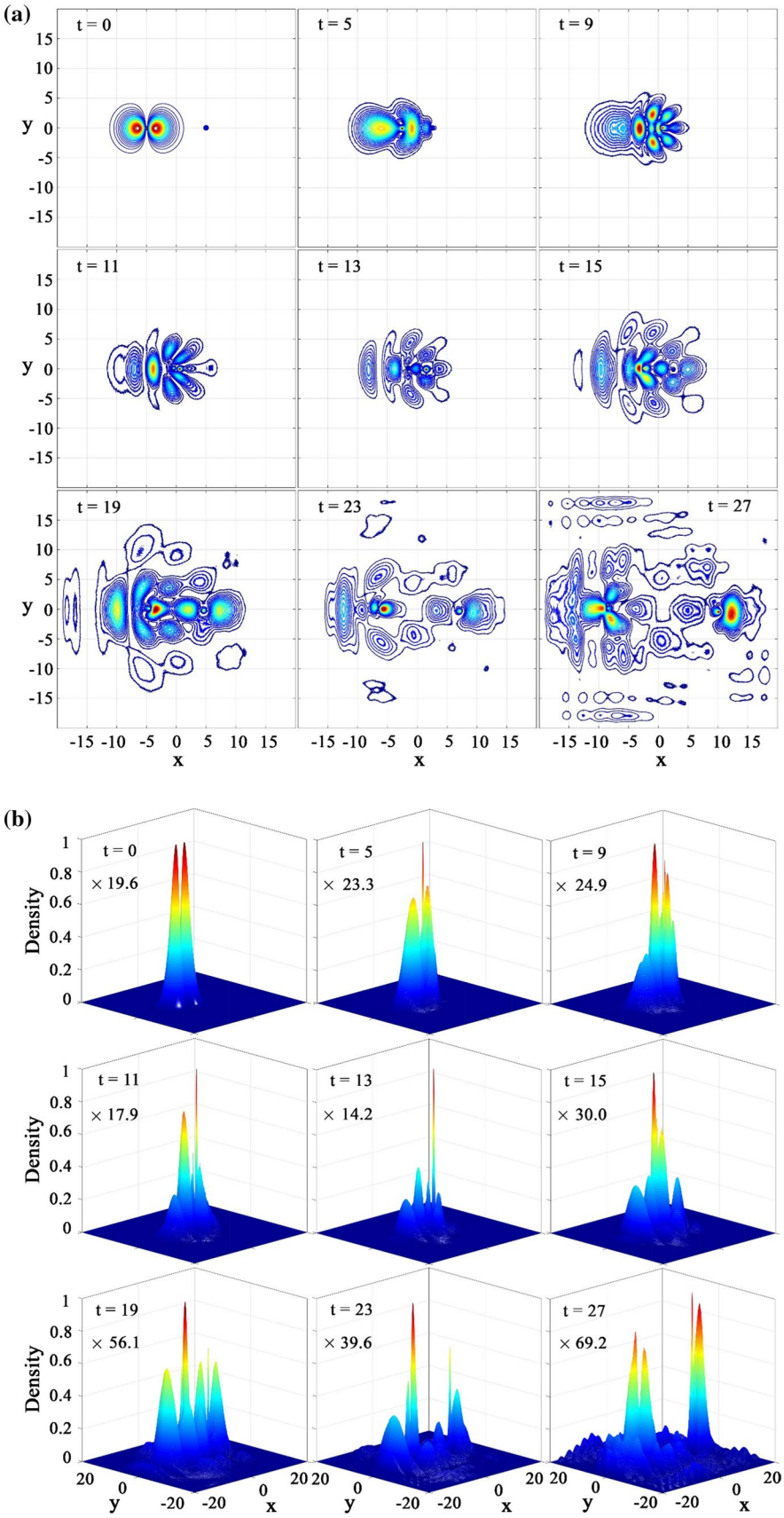

Fig. 4 **a** The same as Fig. 3a but starting from the H-2p_x orbital. **b** The same as Fig. 3b but for the case in which the incoming H atom is in its 2p_x state

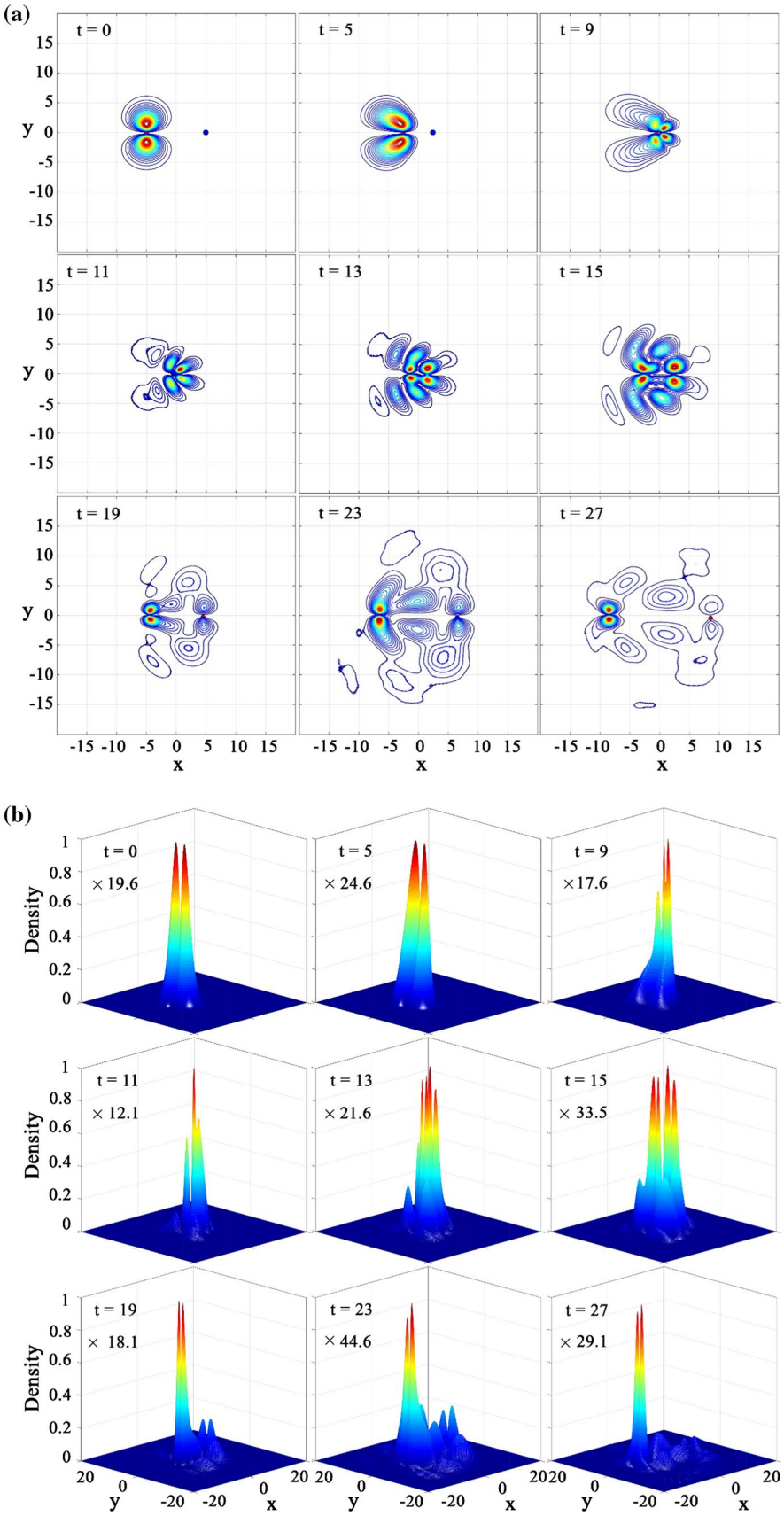

Fig. 5 **a** The same as Fig. 3a but starting from the H-2p_y orbital. **b** The same as Fig. 3b, but for the case starting from the H-2p_y orbital

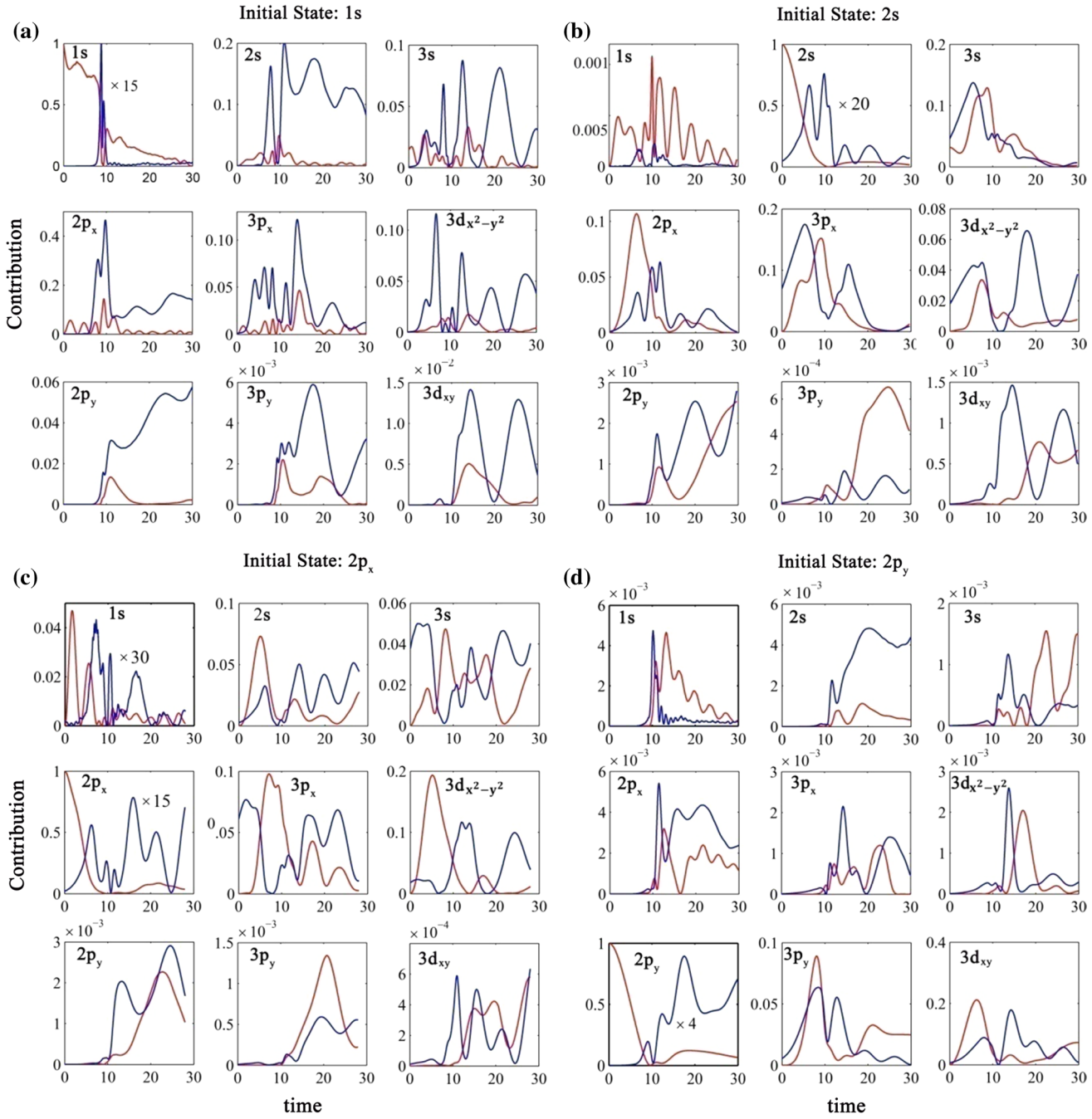

Fig. 6 Coefficients of the expansion of the evolving electron wavepacket in terms of the eigenfunctions of the H and He^+ species during an H-α (H–He^{2+}) collision under the conditions describe in the text and Fig. 1, for the cases in which electron of the incoming H atom is in its different orbitals. **a** 1*s* orbital, **b** 2*s* orbital, **c** $2p_x$ orbital and **d** $2p_y$ orbital

When the incoming H atom is in its 2*s* state, as shown in Fig. 6b, the main electron probability density is transferred initially to the $3p_x$, 3*s* and $2p_x$, and later, it is transferred to the same orbitals of the He^+ species. It is shown in Fig. 6c that the population of the $2p_x$ initial orbital of the H atom is simultaneously transferred mainly to its $3p_x$ and $3d_{x^2-y^2}$ orbitals and to the same orbitals of the He^+ species. Finally, as shown in Fig. 6d, if the initial state of the H atom is $2p_y$ orbital (Fig. 6d), the main contributors to the evolving wavepacket are the $3d_{xy}$, $2p_y$ and $3p_y$ orbitals of both H and He^+ species.

Figure 6 shows that populations of the original 2*s*, $2p_x$ and $2p_y$ orbitals of H atom drop quickly prior to the collision. Also, population of the 2*s* orbital vanishes at the collision time, while those of the $2p_x$ and $2p_y$ are revived

for a short period of time after the collision and then decay to zero. It is also shown in Fig. 6 that time variations of the contribution of the orbitals of the He^+ to the evolving wavepacket are complex. These variations basically depend on the setup of the collision including velocities and the impact parameter as well as the initial state of the H atom. As can be deduced from Fig. 6, sum of contributions are not unity which is due to the limited expansion used in our calculations due to practical limitations.

The net result of this atom–ion collision can be expressed in terms of the transferred probability from the H atom to the He^{2+} nucleus. For this purpose, the simulation box is divided into two partitions by a vertical line passing through the instantaneous electrostatic force null point, r_{null}, which is lied on the internuclear line segment

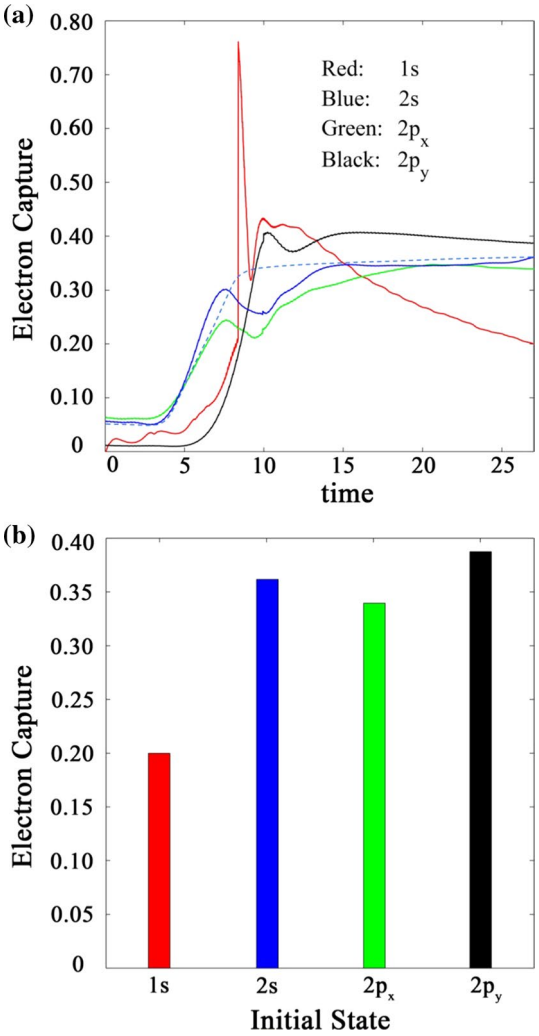

Fig. 7 **a** Time-dependent electron densities captured by the α (He^{2+}) particle from the H atom initially in different orbitals during the H–He^{2+} collision in the simulation box described in Fig. 1. **b** The overall electron densities captured by the α (He^{2+}) particle from the H atom at $t = 27$ au, extracted from part (**a**)

at each time step during the simulation and defined as $f_p(r = r_{null}) = f_\alpha(r = r_{null})$. In this way, the total density of the electron is divided into two ρ_H and ρ_{He^+} densities belonging to the two H and He^+ species, respectively. The ρ_{He^+} value is thus the captured density by the alpha (He^{2+}) particle in this H–He^{2+} collision. Instantaneous values of the captured density are calculated for the four simulations carried out in this research and plotted against time in Fig. 7a. The initial values of ρ_{He^+} should basically be zero. However, as shown in Fig. 7a, these initial values are nonzero for the second layer orbitals. These nonzero values of the ρ_{He^+} are due to the extension of these initial orbitals to the spaces belonged to the alpha particle according to the null point definition discussed above and are not related to the electron capture phenomenon; the more spread the orbital, the larger this initial nonzero value. The instantaneous captured electron densities during simulations corresponding to different initial orbitals of the incoming H atom, plotted in Fig. 7a, show more or less similar behaviors. Furthermore, the first encounter of the H electron density in different orbitals with the α particle, i.e., the rise in the ρ_{He^+} value, follows the order $2p_x < 2s < 1s < 2p_y$ which is a reflection of their orientations (with respect to the collision approach) and extensions in space.

The captured electron density curves corresponding to the $1s$, $2s$ and $2p_x$ show a peak on their rising part prior to the collision time, when the distance between the two (p and α) particles is minimum, then a valley near the collision time and another much smaller peak after the collision time which is more visible for the $1s$ orbital. The captured density curve corresponding to the $2p_y$ orbital shows only one peak after the collision time. In Fig. 7a, all three curves corresponding to the second layer initial orbitals, at the final stage of the simulations, after passing through a valley, increase to their asymptotic values, while the curve of the $1s$ orbital drops significantly after the second peak and reaches its asymptotic value at very late stage ($t \approx 29$ au) of the simulation. By referring to Figs. 3, 4 and 5, it can be concluded that the two peaks observed for the $1s$, $2s$ and $2p_x$ orbitals are due to the passage of the α particle through the dense regions of the orbitals occurring one before and the other after the collision time. Smaller height of the second peak is due to the fact that presence of the α particle near the orbital disturbs the electron probability density toward itself and thus broadens the second dense region arrived after the collision time. Because of the vertical orientation of the $2p_y$ orbital, the α particle meets it at one point only near the collision time, and thus resulting only in one peak in the instantaneous captured electron density curve.

In fact, the peaks observed in the (defined) instantaneous captured electron densities, which show an increase

in the allocation densities to the α particle, are due to the presence of the α particle near the orbitals density regions, while not being able to carry whole of this density away from the proton. Exclusion of this transient feature from the captured electron density curves leaves us with a sigmoid behavior for all four orbitals, plotted in dotted lines in Fig. 7a. For better visualization of the similarities and differences of the effect of initial orbitals on the outcome of H–He^{2+} collision process, the captured electron density at the final stage of the simulation ($t = 27$ au) is extracted from Fig. 7a and plotted as a bar chart in Fig. 7b. According to these data, capture of electron density by the α particle from the hydrogen atom in the four orbitals examined in this work follows the order $1s < 2p_x < 2s < 2p_y$.

Conclusions

The instantaneous and overall captured electron densities by the He^{2+} particle from the H atom during H–He^{2+} collision depend on the impact parameter, relative velocity (energy) and the initial state of the H atom. In this work, the former two parameters are kept fixed (respectively, at 0.1 and 1.0 au) and the effect of the latter is studied by considering the $1s$, $2s$, $2p_x$ and $2p_y$ orbitals of the H atom as the initial state. The results of this research are summarized into three categories: (1) qualitative results of the electron transfer process (Figs. 2, 3, 4, 5), (2) tracking evolution of the wavepacket in terms of the contributing orbitals form the two donor (H) and acceptor (He^{2+}) species (Fig. 6) and finally (3) quantitative results expressed as the captured electron density (Fig. 7). Qualitative and quantitative differences observed in the electron transfer process when starting with different initial states for a certain collision setup can be attributed to the differences in their compactness, shape and orientation (determined by n, l and m_l quantum numbers, respectively). For the H-$1s$ initial orbital, the transfer of electron density occurs at very short internuclear distances near the collision center, and scattering probability is much smaller than those of the other orbitals, while for the second layer $2s$, $2p_x$ and $2p_y$ orbitals, electron density transfer starts at longer internuclear distances (i.e., at earlier times) and the scattering probability is high so that the wavepacket electron density spreads over the entire simulation box after the collision in the occurrence time order of $1s < 2p_y < 2p_x < 2s$. It is found also that although presence of the α (He^{2+}) particle is sensed even at the early stage of the simulation, significant evolution in the electron density distribution occurs at later times according to the order $1s < 2p_y < 2p_x \approx 2s$ (compare parts (b) of Figs. 2, 3, 4, 5). In addition, lagging of electron density, with different scales, is evident for all initial orbitals due to the velocity setup in these simulations. Figure 6 gives us a good view of the state-to-state trajectory history of the electron wavepacket density based on the contributions of different stationary orbitals located on the moving nuclei during the course of the collision process. The electron capture process is described quantitatively in Fig. 7. For example, we can conclude that at $t = 27$ au, electron capture occurs by 0.20, 0.36, 0.34 and 0.39 probabilities when starting, respectively, with the $1s$, $2s$, $2p_x$ and $2p_y$ orbitals of the H atom. Finally, electron transfer, as a probabilistic quantum mechanical process, should be expressed in terms of time-dependent probabilities measured in terms of instantaneous and overall transferred or captured electron densities. Inspection of the evolution of the electron of the hydrogen atom during the encounter with the α particle shows that electron crawls from one nucleus to the other during the electron transfer process.

References

1. J. Jortner, M. Bixon, *Advances in Chemical Physics, Electron Transfer-from Isolated Molecules to Biomolecules*, vol. 106 (Wiley, New York, 2009)
2. A.M. Kuznetsov, J. Ulstrup, *Electron Transfer in Chemistry and Biology: An Introduction to the Theory* (Wiley, New York, 1999)
3. L. Flamm, R. Schumann, Ann. Phys. **355**, 655 (1916)
4. G. Henderson, Proc. R. Soc. Lond. A Math. Phys. Sci. **102**, 496 (1923)
5. E. Rutherford, Philos. Mag. Ser. **6**(47), 277 (1924)
6. J. Jacobsen, Nature **117**, 858 (1926)
7. V. Balzani, *Electron Transfer in Chemistry* (Wiley, New York, 2001)
8. R.E. Blankenship, *Molecular Mechanisms of Photosynthesis* (Wiley, New York, 2013)
9. R.A. Marcus, N. Sutin, Biochim. Biophys. Acta **811**, 265 (1985)
10. V.A. Benderskii, D.E. Makarov, C.A. Wight, *Chemical Dynamics at Low Temperatures*, vol. 188 (Wiley, New York, 2009)
11. J. Cowan, J. Biol. Inorg. Chem. **3**, 195 (1998)
12. H. Lund, K. Daasbjerg, T. Lund, S.U. Pedersen, *Electron Transfer in Some Nucleophilic Reactions. Macromolecular Symposia* (Wiley, New York, 1998)
13. V. Benderskii, V. Goldanskii, D.E. Makarov, Phys. Rep. **233**, 195 (1993)
14. B. Bransden, M. McDowell, E.J. Mansky, Phys. Today **46**, 124 (1993)
15. D. Dewangan, J. Eichler, Phys. Rep. **247**, 59 (1994)
16. J. Eichler, *Lectures on Ion-Atom Collisions: From Nonrelativistic to Relativistic Velocities* (Gulf Professional Publishing, Boston, 2005)
17. H. Sabzyan, M. Jenabi, J. Chem. Phys. **144**, 134306 (2016)
18. M. Machholm, C. Courbin, J. Phys. B At. Mol. Opt. Phys. **27**, 4703 (1994)
19. A.D. Bandrauk, H. Shen, Chem. Phys. Lett. **176**, 428 (1991)
20. A.D. Bandrauk, H. Shen, J. Chem. Phys. **99**, 1185 (1993)
21. M. Feit, J. Fleck, J. Chem. Phys. **78**, 301 (1983)
22. M. Feit, J. Fleck, A. Steiger, J. Comput. Phys. **47**, 412 (1982)
23. M. Feit, J. Fleck Jr., J. Chem. Phys. **80**, 2578 (1984)
24. M. Suzuki, Phys. Lett. A **113**, 299 (1985)
25. R.P. Feynman, Phys. Rev. **84**, 108 (1951)
26. A.D. Bandrauk, H. Lu, J. Theor. Comput. Chem. **12**, 1340001 (2013)

27. C.S. Lent, *Learning to Program with MATLAB: Building GUI Tools* (Wiley, New York, 2013)
28. L. Verlet, Phys. Rev. **159**, 98 (1967)
29. U. Riss, H.-D. Meyer, J. Phys. B At. Mol. Opt. Phys. **28**, 1475 (1999)
30. U. Riss, H.D. Meyer, J. Chem. Phys. **105**, 1409 (1996)
31. P. Sigmund, *Particle Penetration and Radiation Effects Volume 2: Penetration of Atomic and Molecular Ions*, vol. 179 (Springer, Berlin, 2014)
32. X. Yang, S. Guo, F. Chan, K. Wong, W. Ching, Phys. Rev. A **43**, 1186 (1991)